Available online at www.sciencedirect.com
ScienceDirect
Journal of Power Sources 167 (2007) 349–357
JOURNAL OF POWER SOURCES
www.elsevier.com/locate/jpowsour

Monodimensional modeling and experimental study of the dynamic behavior of proton exchange membrane fuel cell stack operating in dead-end mode

Ph. Moçotéguy [a], F. Druart [a,*], Y. Bultel [a], S. Besse [b], A. Rakotondrainibe [b]

[a] *Laboratoire d'Electrochimie et de Physico-Chimie des Matériaux et des Interfaces (LEPMI), UMR 5631 CNRS-INPG-UJF, ENSEEG, BP 75, 38402 Saint Martin d'Hères, France*
[b] *Helion Fuel Cells, Domaine du Petit Arbois, Bâtiment Jules Verne, BP71, 13545 Aix en Provence Cedex 4, France*

Received 10 October 2006; received in revised form 19 January 2007; accepted 5 February 2007
Available online 21 February 2007

Abstract

The dynamic behavior of a five cells proton exchange membrane fuel cell (PEMFC) stack operating in dead-end mode has been studied at room temperature, both experimentally and by simulation. Its performances in "fresh" and "aged" state have been compared. The cells exhibited two different response times: the first one at about 40 ms, corresponding to the time needed to charge the double-layer capacitance, and the second one at about 15–20 s. The first time response was not affected by the ageing process, despite the decrease of the performances, while the second one was. Our simulations indicated that a high amount of liquid water was present in the stack, even in "fresh" state. This liquid water is at the origin of the performances decrease with ageing, due to its effect on decreasing the actual GDL porosity that in turn cause the starving of the active layer with oxygen. As a consequence, it appears that water management issue in a fuel cell operating in dead-end mode at room temperature mainly consists in avoiding pore flooding instead of providing enough water to maintain membrane conductivity.

Keywords: Proton exchange membrane fuel cell; Water management; Dead-end mode; Stack performance; Startup; Dynamic behavior

1. Introduction

As schematically fuel cell assembly shown in Fig. 1, a proton exchange membrane fuel cell (PEMFC) consists of two electrodes containing a thin layer of catalyst in contact with a plastic membrane separating gas supply chambers. The electrodes are constituted by a gas diffusion layer (GDL) and an active layer (AL). The GDL is usually made of carbon cloth, carbon powder and PTFE, while AL usually consists in a Pt/C powder uniformly agglomerated with Nafion® ionomer. Both layers have a porous structure. This assembly is sandwiched between two current collectors [1].

At the anode side, hydrogen gas which acts as fuel is oxidized according to the following reaction:

$$H_2 \rightarrow 2H^+ + 2e^- \quad (1)$$

Similarly, oxygen enters the fuel cell at the cathode where it is reduced in water according to the following reaction:

$$O_2 + 4H^+ + 4e^- \rightarrow 2H_2O \quad (2)$$

Gaseous oxygen fed in the gas channel diffuses through the GDL and in the pores of the AL, where it dissolves in Nafion® on the surface of the agglomerates. Dissolved oxygen diffuses towards the centre and reacts on the numerous Pt particles. The management of the water generated by reaction (2) remains a major issue. On one hand, its shortage causes a dehydration of the ionomer which in turn generates an increase of the cell's resistance due to the decrease of protons mobility inside the ionomer. On the other hand, its excess causes pores flooding by liquid water that hinders oxygen diffusion in the porous volumes of both the GDL and the AL [1]. Modeling could be a useful tool

* Corresponding author at: LEPMI, ENSEEG, Domaine Universitaire, BP 75, 38402 Saint Martin d'Hères, France. Tel.: +33 476826733; fax: +33 476826777.
E-mail addresses: philippe.mocoteguy@enseeg.inpg.fr (Ph. Moçotéguy), florence.druart@lepmi.inpg.fr (F. Druart), yann.bultel@lepmi.inpg.fr (Y. Bultel), serge.besse@helion-fuelcells.com (S. Besse), andre.rako@helion-fuelcells.com (A. Rakotondrainibe).

0378-7753/$ – see front matter © 2007 Elsevier B.V. All rights reserved.
doi:10.1016/j.jpowsour.2007.02.028

Nomenclature

[]	concentration (mol m^{-3})
C	capacitance (F m^{-2})
D	diffusion coefficient (m^2 s^{-1})
F	Faraday constant (C mol^{-1})
j	current density (A m^{-2})
M	molar mass (g mol^{-1})
n	number of moles
P	pressure (Pa)
R	resistance (Ω)
$\mathcal{R}$	Gas constant (J K^{-1} mol^{-1})
s	volume fraction of water in the GDL
S	geometrical surface area (m^2)
t	time (s)
T	temperature (K)
U	cell voltage (V)
V	volume (m^3)
x	distance in direction orthogonal to electrode surfaces (m)

Greek symbols

δ	GDL thickness (m)
ε	porosity
η	overvoltage (V)
ρ	volumetric mass (kg m^{-3})

Subscripts

0	initial
act	reactive
AL	active layer
C	capacitive
dl	double layer
dry	in dry state
e	electrode
eff	effective
eq	equilibrium
exp	experimental
F	Faradaic
GDL	gas diffusion layer
int	internal
imp	imposed
sat	saturation

for the improvement of the water management, since it allows a better understanding of its effect on fuel cell performances.

The cell would be operated on 100% hydrogen and oxygen utilization, i.e. on a stoichiometry of 1. This is also referred to as "dead-end" operating mode. From the system point of view, dead-end operation can be accomplished by closing the gas outlet of the cell.

In the past, the mathematical models of the PEMFC were usually restricted to the steady state conditions and transient models only recently appeared. But these models are so far restricted to stoichiometric mode. Bernardi [2] first proposed a one-dimensional model in order to study the water management and to identify the humidification conditions which induce either the dehydration of the membrane or excessive flooding. The sensitivity to the water balance of the PEMFC performance was demonstrated. Some other models were derived from the original one to take into account heat management [3], mass transport in the gas diffusion electrode [4] or to introduce a different treatment of the electrochemical reaction [5]. Bernardi et al. [6] and Springer et al. [7] also presented a one-dimensional model to investigate the factors that limit cell performance and to elucidate the mass transport mechanism within the complex network of gas, liquid and solid phases constituting the gas diffusion electrode. Contrary to the previous models, this latter one considered the molar changes along the gas channel. These approaches made it possible to evaluate the losses in the cathode gas backing and the catalyst layer.

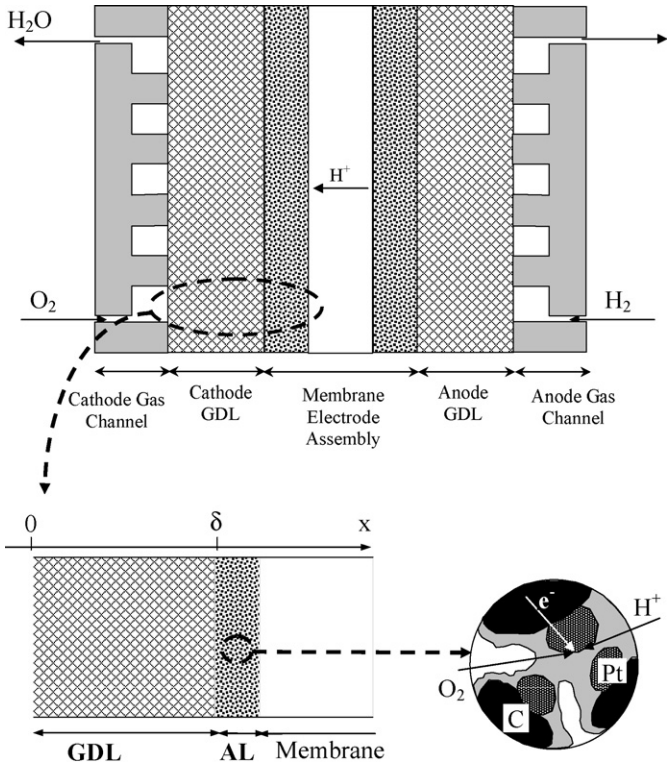

Fig. 1. Schematic representation of a PEMFC and the gas diffusion electrode.

So far, efforts have been made to model the problem in three dimensions. A higher dimensionality makes it possible to describe the hydrodynamics and multi-component transport inside the flow channel for reactant distribution. Multi-component models were thus developed for cathode or for whole PEMFC, for both single-phase [8] and two phase flow [9]. These models showed that the gas distributor geometry has a significant effect on the diffusion of the reactants and products in determining the performance of the cell. Moreover, they confirmed that the performance of cathode is strongly influenced by the presence of liquid water and its removal rate, especially at high current density.

The dynamic study of a fuel cell appears to be of great interest to provide detailed understanding of mass and charge transport

through the gas diffusion electrodes and is of extreme importance for the control strategy and system management in power generation systems, especially when there are power injections into the network. Thus, a first equivalent circuit was proposed to simulate the impedance spectrum of a PEMFC [10]. This study showed that the impedance of a fuel cell is a powerful tool in order to characterize the intra-electrode processes occurring in gas diffusion electrodes.

Many recent dynamic models of PEMFC [9,11–19] have been developed, based on the physical and chemical knowledge of the phenomena occurring inside the cell. Some of them even take into account the multi-dimensional geometry of the cell [9,18,19] while some others exhibited an important effect of water management [13–15]. Ceraolo et al. [11] provided the static and dynamic model of PEMFC. Their one-dimensional model only considered the cathode side, and the transient terms were added to the species balance and phase potential equation. They obtained a good correlation between their numerical predictions and experimental results. Yerremalla et al. [12] proposed a dynamic model based on semi-empirical equations. In contrast, the model of Wang and Wang [14] includes the full description of water and proton co-transport in the three-dimensional MEA, thus it could provide detailed information of water behaviors in this vital component, such as water accumulation. It is found that membrane hydration occurs over a period of 10 s, the gas transport of 0.01–0.1 s, with the double-layer discharging being negligibly fast. Some other models were developed in a more "System" approach [20]. These models are relatively simple which allow correctly simulating the behavior of the fuel cell inserted in an electrical network. The main disadvantage of these models is that they are far away from the physics of the fuel cell, i.e. their parameters are physically non-representative. In parallel, some other multi-scale models were elaborated [21] to predict the dynamic and steady state behaviors for the triple contact (where the electrochemical reaction proceeds). These models made it possible to describe quantitatively the reaction mechanisms, the polarization curves and impedance spectra of the fuel cell. However, all these models deal with a cell operating in stoichiometric mode and little attention has been paid to systems that operate in dead-end mode.

In addition, few experimental studies of dynamic behavior of the PEMFC were performed, all related with operation in stoichiometric mode with changes between two operating regimes [11,13,22–24]. None of these works deals with the starting behavior of a PEMFC operating in dead-end mode or studied the transient behavior to a step current/voltage from open circuit voltage (OCV). Kim et al. thus studied, using a two channel digital oscilloscope, the influence of stoichiometry [22], reservoirs and fuel dilution [23], flow field design and voltage step magnitude [24] on the dynamic behavior of PEMFC operating in stoichiometric mode. Their results indicate that the response time to a step voltage was ranging between 3 s for a change in operation from excess to normal stoichiometry to 15 s for a change in operation from starved to normal stoichiometry [22]. All these studies, depending on the operating conditions, show either undershoot (transient current below the steady state value) or overshoot (transient current above the steady state value) behavior usually attributed to local changes in the polymer electrolyte conductivity caused by the change in local water content in the vicinity of the reactive sites [11].

In this paper, the authors have focused on the dynamic modeling of the transient response of a PEMFC stack operating in dead-end mode. So as to better understand this dynamic behavior, we studied both experimentally and numerically the starting performances of such cells. The experimental results were compared, in the first ten seconds of operation, with the prediction of a simple mono-dimensional model of the transient behavior. In addition, the model's ability to predict the voltage level and the time response of the fuel cell was evaluated.

2. PEMFC dynamic model

2.1. Basic assumptions

A dynamic one-dimensional PEMFC model is developed to predict the transient response of the PEMFC to a step current. So, a dynamic model of PEMFC capable of characterizing transient phenomena is proposed which incorporates simultaneously the prominent dynamic aspects occurring within the GDL and electrochemical double-layer charge or discharge. Based on the basic consideration reported in the literature, the main assumptions of the proposed model are as follows:

(i) The influence of the anode side of the PEMFC on its transient behavior was neglected, due to on one hand the faster kinetics of the hydrogen oxidation reaction with regard to the kinetics of oxygen reduction reaction [18], and on the other hand, to the faster diffusion of hydrogen gas in the anodic GDL with regard to the diffusion of oxygen on the cathodic side [25,26].

(ii) Due to the small time periods considered in this model, the system was considered isothermal. The study was focused on PEMFC starting performances at room temperature.

(iii) The water vapor pressure in the gas phase was considered as constant and fixed to its saturation value. This later hypothesis is reasonable as we consider a fuel cell operating at room temperature. The water produced by the electrochemical reaction was thus considered in liquid state and its effect was taken into account through an homogeneous decrease of the GDL porosity ε, according to the following equation [27]:

$$\varepsilon = \varepsilon_{\text{dry}}(1 - s) \tag{3}$$

where ε_{dry} and s, respectively, correspond to the GDL porosity in dry state and to the GDL water content (volume fraction of water inside the pores of the GDL).

In addition, we also assumed that this liquid water partly blocks the electrode geometrical surface area S_e, reducing the reactive area S_{act} with a magnitude proportional to its volume fraction, according to the following relation:

$$S_{\text{act}} = S_e(1 - s) \tag{4}$$

(iv) The gas transport in the GDL was assumed to obey Fick's law and an ideal gas mixture is considered.
(v) Electrodes were considered as a planar interface at which reaction proceeds. The complex structure of the AL and the distribution of the reaction in its volume were not taken into account.
(vi) The PEMFC was considered as operating in dead-end mode, at a fixed gas pressure, with periodic short bleeds. But, due to the short period of time considered in this study, no bleed was taken into account in our model.
(vii) Due to the small time periods considered in this model, the membrane water content was assumed to be constant and no electro-osmotic flux or water diffusion flux was taken into account.

2.2. Gas mass balance equation

The oxygen entering the cell before reaching the catalyst layer diffuses, through the gas diffusion layer, within a gaseous mix constituted by water vapor and oxygen itself. This phenomenon is described by the equation of continuity for oxygen gas:

$$\frac{\mathrm{d}[\mathrm{O_2}]}{\mathrm{d}t} - \frac{\mathrm{d}}{\mathrm{d}x}\left(D_{\mathrm{eff,O_2}}\frac{\mathrm{d}[\mathrm{O_2}]}{\mathrm{d}x}\right) = 0 \tag{5}$$

where $D_{\mathrm{O_2,eff}}$ is the effective oxygen diffusion coefficient in the porous medium, that can be determined from the oxygen diffusion coefficient in free medium $D_{\mathrm{O_2}}$ and from medium's porosity ε, according to the Bruggeman equation [28]:

$$D_{\mathrm{O_2,eff}} = D_{\mathrm{O_2}}\varepsilon^{1.5} \tag{6}$$

And according to ideal Gas law:

$$P_{\mathrm{O_2}} = \frac{n_{\mathrm{O_2}}}{V}\mathcal{R}T = [\mathrm{O_2}]\mathcal{R}T \tag{7}$$

Therefore, Eq. (5) can be rewritten as follow:

$$\frac{\mathrm{d}P_{\mathrm{O_2}}}{\mathrm{d}t} - D_{\mathrm{eff,O_2}}\frac{\mathrm{d}^2P_{\mathrm{O_2}}}{\mathrm{d}x^2} = 0 \tag{8}$$

This mass balance equation has to be solved in the respect of the following boundary conditions:

(i) At gas channel/GDL interface, the oxygen pressure is constant equal to the cathode pressure minus the water saturation pressure:

$$P_{\mathrm{O_2}}(x=0) = P_0 - P_{\mathrm{H_2O,sat}} \tag{9}$$

(ii) At electrode/GDL interface, the oxygen flow rate is directly related to the Faradaic current j_{F}, according to the Faraday's law:

$$-D_{\mathrm{O_2,eff}}\frac{\mathrm{d}P_{\mathrm{O_2}}}{\mathrm{d}x}(x=\delta) = -\frac{\mathcal{R}T}{4F}j_{\mathrm{F}}. \tag{10}$$

The Faradaic current can be related to the overvoltage at the interface, η, through an approximated formulation of the Butler–Volmer equation, already used in the literature [11,16]:

$$j_{\mathrm{F}} = -j_{\mathrm{eq}}\left(\frac{P_{\mathrm{O_2}}(x=\delta)}{P_{\mathrm{O_2}}(x=\delta,\, j=0)}\,\mathrm{e}^{(F/2\mathcal{R}T)\eta} - 1\right)$$
$$= -j_{\mathrm{eq}}\left(\frac{P_{\mathrm{O_2}}(x=\delta)}{P_{\mathrm{O_2}}(x=0)}\,\mathrm{e}^{(F/2\mathcal{R}T)\eta} - 1\right) \tag{11}$$

In Eq. (11), the number of electron involved in the reaction is equal to 1, while value of 4 would have been expected according to reaction (2). However, Parthasarathy et al. [29] have shown that, whatever the temperature in the range 30–80 °C, the oxygen reduction reaction at platinum/Nafion® interface proceeds with two different mechanisms, depending on the applied current density. For fuel cell current densities above 10^{-2} A cm^{-2}, a reaction rate in first order with respect to O_2 pressure was observed indicating a single electron transfer reaction. This behavior was reported to be linked with a reaction that proceeds on a Pt-oxide free surface [29].

2.3. Charge balance equation at the cathode/GDL interface

An electrostatic electrical equilibrium is established at a metal electrode/electrolyte (Nafion®) interface resulting in a so-called "double layer" of separated negative (electrons inside the metal catalyst) and positive charges (protons in the Nafion®) across the interface [30]. The interface behaves like a capacitor in which the charge density of electrons and ions at the interface depends on the potential difference across this double layer. As a result, when a current is set to a cell, the operating voltage shows an immediate change due to the internal resistance, usually called "ohmic drop", and then evolves slowly as double-layer capacitance (C_{dl}) is charged/discharged and electrochemical reaction proceeds simultaneously. The set current is thus split in a capacitive current j_{C} "used" to charge/discharge the double-layer capacitance and in a Faradaic current j_{F}, "used" to perform the electrochemical reaction [30].

Moreover, the capacitive current is unaffected by the liquid water present in the gaseous pore since charges accumulate of both sides of platinum particles/ionomer interface which are not impacted by liquid water. Oppositely, the Faradaic current is affected by the flooding of the gas pores because the access of oxygen gas to the active particles is hindered. As a consequence, the charge balance equation can be written as follow:

$$j_{\mathrm{imp}}S_{\mathrm{e}} = j_{\mathrm{C}}S_{\mathrm{e}} + j_{\mathrm{F}}S_{\mathrm{act}} \Leftrightarrow j_{\mathrm{imp}} = C_{\mathrm{dl}}\frac{\mathrm{d}\eta}{\mathrm{d}t} + j_{\mathrm{F}}(1-s) \tag{12}$$

where j_{imp} is the imposed current density.

The overvoltage evolution resulting from a step current can thus be calculated as follows:

$$\frac{\mathrm{d}\eta}{\mathrm{d}t} = \frac{j_{\mathrm{imp}} - j_{\mathrm{F}}(1-s)}{C_{\mathrm{dl}}} \tag{13}$$

The operating voltage evolution following a current step can in turn be calculated as follow:

$$U(t) = U_{\mathrm{OCV}} - R_{\mathrm{int}}j_{\mathrm{imp}}S_{\mathrm{e}} - \eta(t) \tag{14}$$

2.4. Water balance equation

If all produced water is considered to condensate in the GDL, homogeneously reducing its porosity, the change of the water content in the GDL is expressed from the Faradaic current:

$$\frac{\rho_{H_2O}}{M_{H_2O}}\varepsilon_{dry}V_{GDL}\frac{ds}{dt} = \frac{j_F S_{act}}{2F} \quad (15)$$

2.5. Initial conditions

This approach has been developed to simulate the dynamic response of the cell potential to a steep change of the current density from 0 to 0.5 A cm^{-2}. So, we focused on the starting behavior of the fuel cell. As a consequence, the initial conditions are zero current and voltage equals the OCV. When no current passes in the cell, the oxygen pressure is homogeneous and equals the pressure at $x = 0$, as defined by Eq. (9). The initial value of the liquid volume fraction, s_0, is one of the model's parameter.

2.6. Resolution

The GDL was divided in 50 elements in x-direction along its thickness. Eq. (8) was then discretized using a finite difference method. The overvoltage and the water volume fraction changes are calculated according to Eqs. (13) and (15), respectively. There are three adjustable model parameters to fit experimental data: the initial water volume fraction s_0, the equilibrium current density j_{eq} and the double-layer capacitance C_{dl}. The model was solved in two successive steps with Matlab, using the ODE 15S algorithm with the set of constants and parameters reported in Table 1.

Time constants for electrochemical double-layer, and gas transport were reported to occur over a period of 0.01–0.1 s [14]. In the first step, we thus solved the set of Eqs. (3)–(14) with time scale of 0.1 s to determine the voltage evolution associated with oxygen mass transport and double-layer capacitance charge. During this short time period, water accumulation effect was neglected. The value of the liquid fraction was fixed at s_0.

Table 1
Model constants and parameters

Constants	Parameters
$P_0 = 2$ bars $= 2.027 \times 10^5$ Pa	j_{eq} (A m^{-2})
$P_{H_2O,sat} = 1704$ Pa	s_0
$T = 288$ K	C_{dl} (F m^{-2})
$j_{imp} = 5000$ A m^{-2}	
$S = 0.03$ m^2	
$\delta = 3.54 \times 10^{-4}$ m (given by the manufacturer)	
$\varepsilon_{dry} = 0.8$ (given by the manufacturer)	
$D_{O_2} = 1.192 \times 10^{-5}$ m^2 s^{-1} [25]	
$U_{OCV} = 1.05$ V	
$R_{int,fresh} = 1.05 \times 10^{-3}$ Ω	
$R_{int,aged} = 1.3 \times 10^{-3}$ Ω	
$\rho_{H_2O} = 1000$ g L^{-1}	
$M_{H_2O} = 18$ g mol^{-1}	

In the second step, we used the voltage and the pressure profile calculated in the first step as initial conditions. We solved the set of Eqs. (3)–(15), considering that the double-layer capacitance is fully charged and water accumulation was taken into account.

The unknowns that the model determines are the pressure profile inside the GDL, the cell voltage and the water volume fraction.

3. Experimental

The dynamic behavior of a PEMFC stack consisting of five cells with 300 cm^2 active area, developed by Helion company was studied by setting a step current signal (10^7 A s^{-1} rate) from 0 to 150 A (0.5 A cm^{-2}), at a temperature of 288 ± 2 K. Analytical grade hydrogen and oxygen were used in this study as fuel and oxidant.

The fuel cell test bench used in this study was operated by a Schneider Electric Premium system that independently controlled fluidic and electric circuits and guarantee the safety of the experiment (Fig. 2). The stack was fed with dry reactive gases and operated in dead-end mode. The pressure in each compartment was automatically regulated at 2 bars. Current was controlled by an Agilent N3300A electronic load with two N3306A modules (0–120 A, 0–60 V, 600 W). Before applying the current, the stack was swept for at least 2 min with reactive gases and then maintained at operating pressure for a few minutes. When set, current was maintained during 30 s and then steeply shut down. The temperatures of inlet and outlet cells of the stack were measured by thermocouples during the whole experiment and did not increase more than 2 K. Current, total voltage and each cell voltage evolutions were recorded using a Keithley KUSB-3108 data acquisition module, at a 2000 Hz frequency in the first second after the current setup and then at a 5 Hz frequency from 1 to 30 s after the current switch on.

The stack dynamic behavior was first studied just after manufacturing and few hours of conditioning operations, and then after cycling and ageing during 3 months in conditions that cannot be detailed for confidentiality reasons. The former case will

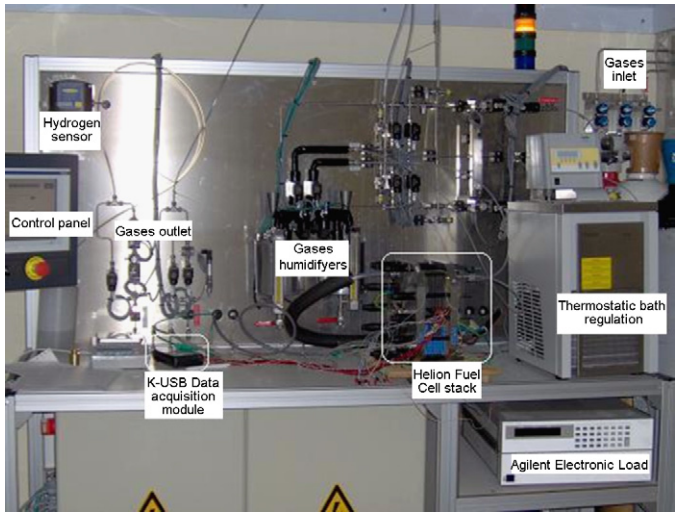

Fig. 2. Test bench.

be referred as "fresh" while the latter case will be referred as "aged".

4. Results

4.1. Experimental results

Fig. 3a and b, respectively, show the dynamic responses of each cell of the fresh and the aged stack to a steep change of the current density from 0 to 0.5 A cm^{-2}. The graphs exhibit three main parts:

(i) During the first second, a rapid decrease of the potential from the OCV (about 1.06 V, not shown on Fig. 3) is observed, followed by an overshoot behavior, with a transient maximum in the cell voltage. Such behavior was already reported in the literature [11,13,22–24]. In addition, the amplitude of this overshoot is magnified by the ageing process: 24 ± 4 mV per cell for the aged stack instead of 10 ± 4 mV per cell for the fresh stack.
(ii) In the range between 1 s and about 15 s, a continuous decrease of the potential is observed.
(iii) After 15 s, an almost steady-state plateau is observed. Beyond 20 s, the cell voltage gradually increases due to the internal temperature increase due to the Joule effect and the exothermic electrochemical reactions. In addition, the period requires to reach the new steady-state is higher for the cell located at the gases outlet than for the other cells: 20 s instead of 15 s. This time strongly depends on the stack's history and appears to be the most critical for the stack's performances.

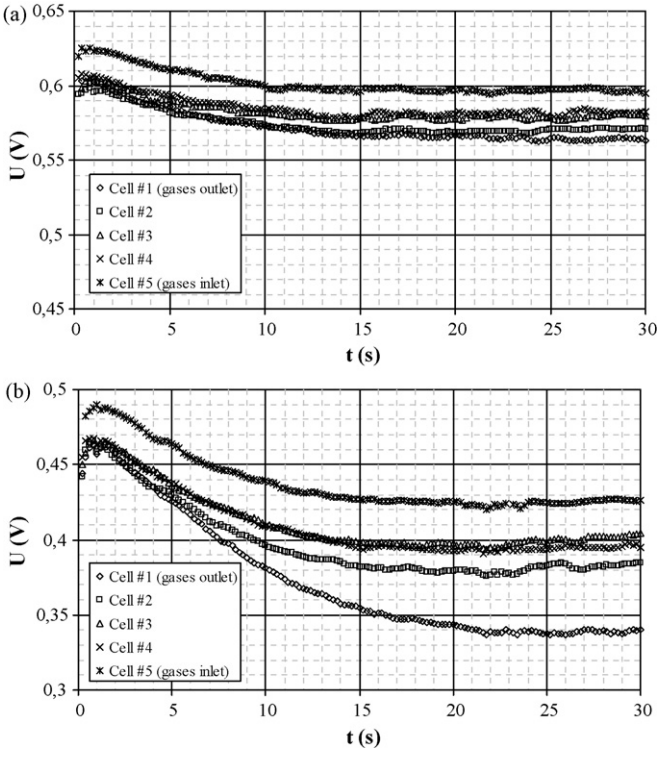

Fig. 3. Evolution of each cell voltage after a current step from OCV: (a) fresh stack and (b) aged stack.

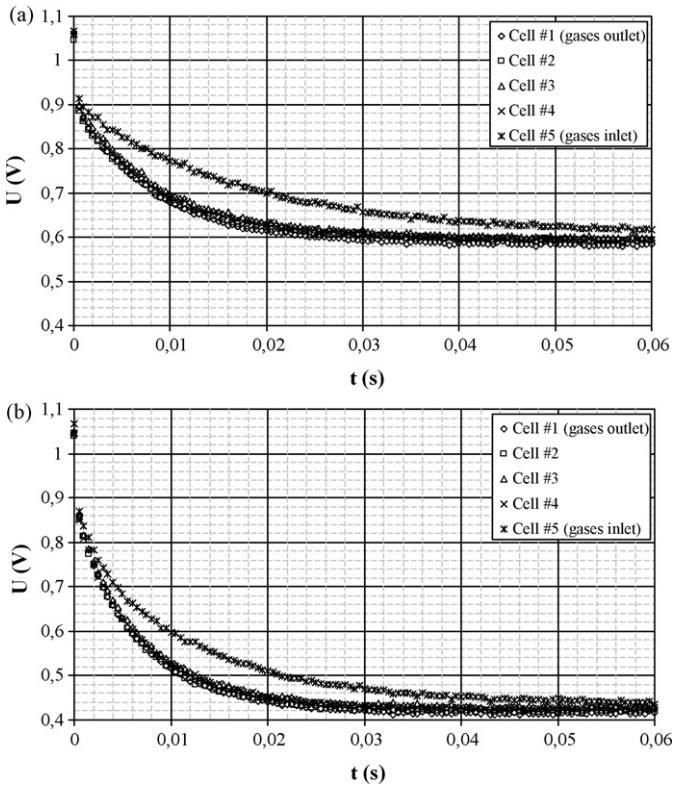

Fig. 4. Evolution of each cell voltage during the first 60 ms after a current step from OCV: (a) fresh stack and (b) aged stack.

It is worth mentioning that the cell at the gases inlet (cell #5) exhibits the best performances while the one at the gases outlet (cell #1) exhibits the lowest performances. So, the voltage difference between the first and the last cell into the stack is about 30 mV for the fresh stack and about 80 mV for the aged stack.

For further investigation, we magnified these evolutions in the first 60 ms after the current step on Fig. 4a and b. This graphs show that the cell voltage reaches a first plateau about 30–40 ms after current switch on. In addition, despite the short time cells performances are strongly decreased by the ageing, corresponding response time is similar for both the fresh and the aged stack.

The data presented in Fig. 4a and b allows us to determine the cells ohmic resistance. Indeed, when an electrochemical cell is submitted to a current step from zero, its voltage first exhibits a steep change due to the ohmic drop. Then, it evolves as Faradaic processes and double-layer capacitance charge/discharge proceed simultaneously, until the latter phenomenon ends [30]. As a consequence, if a fast acquisition system like the one used in this study monitors the voltage evolution, the voltage difference between the last measurement before the current setup and the first measurement after the current setup can provide a good approximation of the cell's ohmic resistance. The shorter the time duration between these measurements is, the better the approximation is. From the data presented in Fig. 4a and b, the

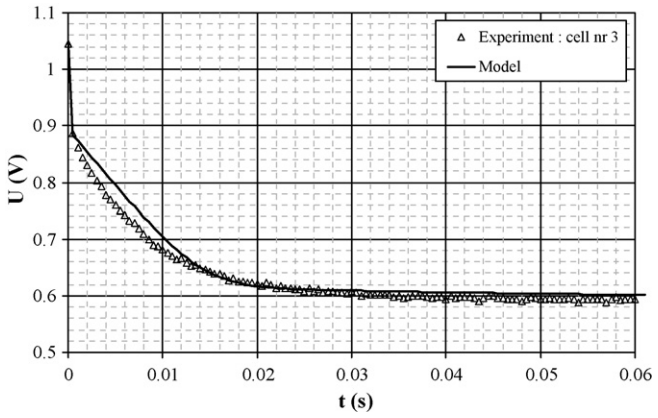

Fig. 5. Evolution of cell voltage during the first 60 ms after the current step, for a fresh stack versus model fitted for $C_{dl} = 254\,F\,m^{-2}$, $j_{eq} = 110\,A\,m^{-2}$ and $s_0 = 0.824$.

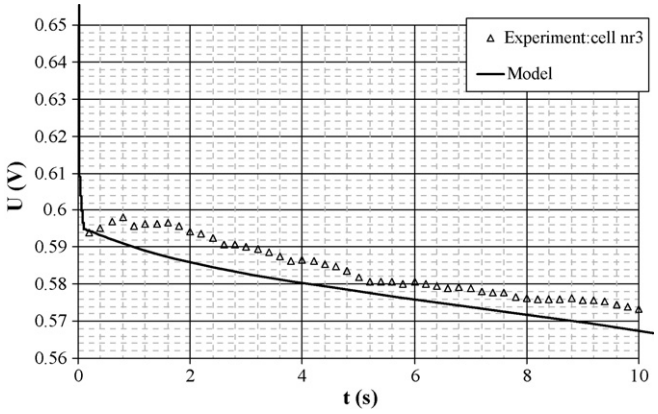

Fig. 6. Evolution of cell voltage during the first 10 s after the current step, for a fresh stack versus model fitted for $C_{dl} = 254\,F\,m^{-2}$, $j_{eq} = 110\,A\,m^{-2}$ and $s_0 = 0.824$.

cell's internal resistance can thus be calculated as follow:

$$R_{int} = \frac{U_{OCV} - U_{t=0.5\,ms}}{j_{imp} S_e} \quad (16)$$

Obtained values for fresh and aged cells were, respectively: 1.05 ± 0.05 and $1.25 \pm 0.05\,m\Omega$. These values were used as input parameters in our model.

4.2. Simulation results

Only three parameters were used to fit the evolutions of the simulated transient response to the experimental results: the initial water volume fraction s_0, the equilibrium current density j_{eq} and the double-layer capacitance C_{dl}. Based on the previous PEMFC dynamic model, a procedure is performed to fit the experimental results obtained for the middle cell (cell #3) of both fresh and aged stack. This cell was chosen because thermal and fluidic edge effects are minimized. The fitting was obtained by a Newton–Raphson algorithm that solves non-linear least square problems, using the Matlab optimization toolbox (LSQCURVEFIT function). For the fitting, the data points corresponding to the overshoot behavior were removed, since our model does not take this phenomenon into account. For consistency, the experimental data points used for the curve fitting in the range 1–10 s were decreased by the magnitude of the observed overshoot. In addition, the experimental data points beyond 10 s were not used for the curve fitting because our model does not take into account the cell temperature increase due to the heat production by the stack that impacts the cell voltage evolution.

Figs. 5 and 6 compare experimental and simulated cell voltage evolutions for the fresh stack, respectively, in the first 60 ms and 10 s after the current step. A very good agreement between experimental and simulated voltage evolutions were obtained for the following set of parameters: $C_{dl} = 254\,F\,m^{-2}$, $j_{eq} = 110\,A\,m^{-2}$ and $s_0 = 0.824$. The observed slight discrepancies can be directly associated with the model assumptions: overshoot behavior and temperature evolution were not taken into account. Interestingly, the corresponding value of s_0 is about 80%, indicating that a high amount of liquid water is already present in the GDL before starting the cell [31].

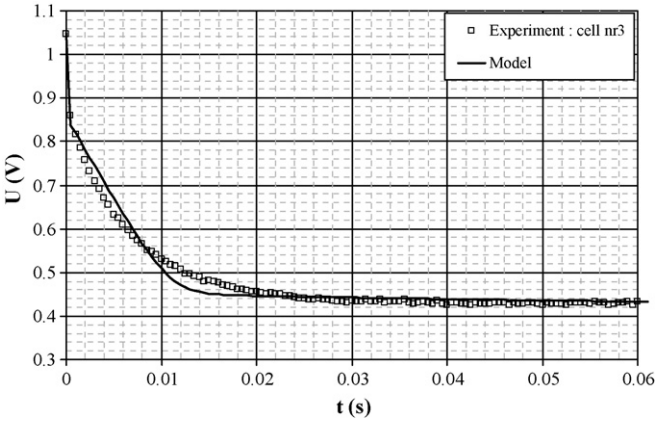

Fig. 7. Evolution of cell voltage during the first 60 ms after the current step, for a aged stack versus model fitted for $C_{dl} = 135\,F\,m^{-2}$, $j_{eq} = 10\,A\,m^{-2}$ and $s_0 = 0.845$.

Figs. 7 and 8 compare experimental and simulated cell voltage evolutions for the aged stack, respectively, in the first 60 ms and 10 s after the current step. The model provides a good prediction of the cell's time response and voltage level for the following set of parameters: $C_{dl} = 135\,F\,m^{-2}$, $j_{eq} = 10\,A\,m^{-2}$

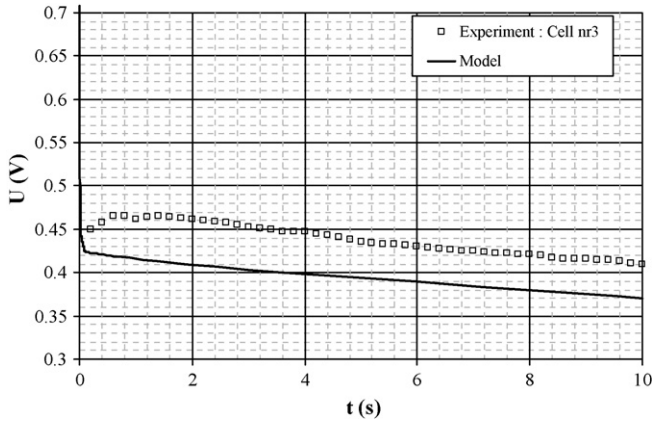

Fig. 8. Evolution of cell voltage during the first 10 s after the current step, for a aged stack versus model fitted for $C_{dl} = 135\,F\,m^{-2}$, $j_{eq} = 10\,A\,m^{-2}$ and $s_0 = 0.845$.

and $s_0 = 0.845$. A higher value of the initial liquid water content s_0 is required to fit experimental cell potential change in the case of the aged stack. This means that water management becomes more and more drastic to maintain acceptable performances. These results are in accordance with those obtained by Pasaogullari and Wang [32] who explained the decrease of PEMFC performances by the formation of liquid water in the cathode. This liquid water in the pore walls may reduce the effective pore size available for gas motion leading to an increase of the mass transport limitations.

The double-layer capacitance values (for the all electrode surface: 300 cm^2) obtained from these fitting were 7.62 and 4.06 F for the fresh and the aged stack, respectively. Such decrease in the double-layer capacitance seems to indicate that the AL is affected by the ageing process. From these values, we can estimate the very minimum time necessary to charge the double-layer capacitance assuming that all the applied current is used for that. Indeed, as previously explained, after the steep change due to the ohmic drop, the voltage evolves as Faradaic processes and double-layer capacitance charge/discharge proceed simultaneously, until the latter phenomenon ends and the voltage stabilizes. Thus, by setting $j_F = 0$ in Eq. (13) and using experimental values from Figs. 5 and 7, the values of the very minimum time needed to charge the double-layer capacitance can be calculated as follow:

$$dt = \frac{C_{dl}}{j_{imp}}(U_{0.5\,ms} - U_{0.06\,s}) \quad (17)$$

Obtained values were 15.3 and 10.9 ms for the fresh and the aged stack, respectively. This validates at posteriori the time limit of 0.1 s we have chosen in our calculation, beyond which the double-layer capacitance was considered as charged.

Fig. 9 compares the evolutions of the calculated Faradaic and capacitive currents, for the aged and the fresh stack. This graph clearly shows that the double-layer capacitance is charged faster in the aged stack than in the fresh stack. But, in both cases, the time needed to charge this double-layer capacitance is lower than 40 ms, and this is consistent with the time limit of 0.1 s chosen in our calculation.

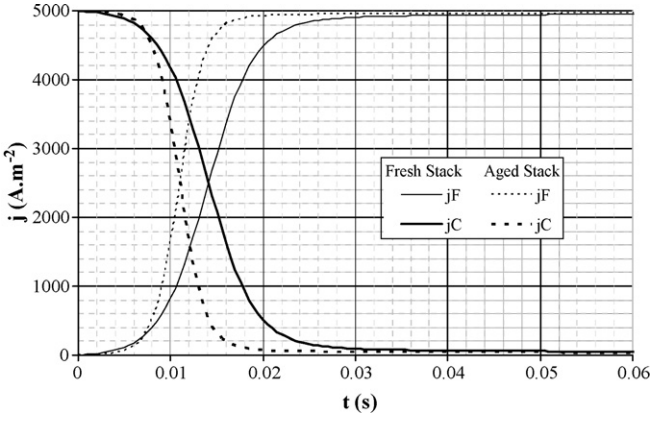

Fig. 9. Comparison between the simulated evolutions of the Faradaic and the capacitive currents of the fresh and the aged stacks.

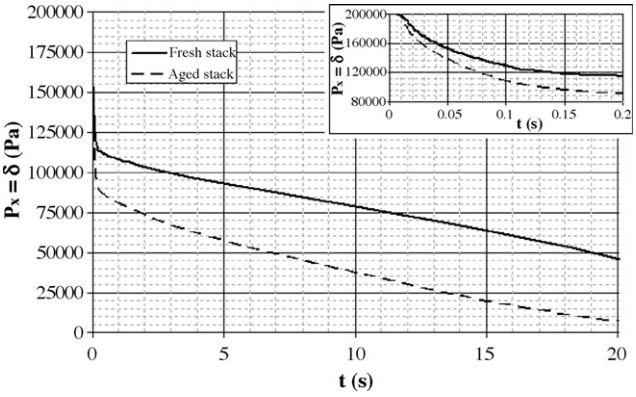

Fig. 10. Comparison between the simulated evolutions of the oxygen interfacial pressure in the fresh and the aged stacks.

Fig. 10 compares the evolutions of the simulated oxygen pressure at the GDL/electrode interface for both fresh and aged stack. We notice that an induction period of about 10 ms is predicted by the model as the double-layer capacitance has begun to charge. Then, oxygen interfacial pressure decreases as an increasing part of the current is used to perform the electrochemical reaction. Then, the interfacial pressure evolution exhibits another time constant at about 150 ms, after which the interfacial partial pressure has decreased by 40% in the case of the fresh cell and by 51% in the case of the aged cell. This indicates that the oxygen reduction reaction rapidly becomes mass transfer limited. In addition, the model predicts that the electrode/GDL rapidly operates in starved oxygen conditions: the predicted interfacial pressure has decreased to 5×10^4 Pa after 7 and 19 s of operation, for the aged and the fresh stack, respectively and to 2.5×10^4 Pa after 14 s of operation in the aged stack. In both cases, a linear decrease of the interfacial oxygen pressure with time is observed beyond 200 ms of operation. This corresponds to the linear increase of the liquid water volume fraction that can be calculated from Eq. (15) at a 0.165% s^{-1} rate.

5. Discussion

The influence of the position of the cell in a stack operating in dead-end mode on its performances can be explained by two simultaneous phenomena: a water accumulation toward the outlet of the stack and a higher reactant gases partial pressure at the inlet of the stack. This is the consequence of the operating mode chosen for this study. Indeed, in dead-end mode, the gases are fed on one hand of the cell and their pressures are regulated on the basis of the value measured at stack's inlet. And, whatever the quality of the gas distribution system within the stack, there is a pressure gradient between the cells located at both ends of the stack. The fed gases are progressively consumed by the cells located at the stack's upstream while produced water progressively accumulates at the stack's downstream, pushed by the inlet gases velocity. This can explain why the cell located at gas inlet exhibits better performances than the one located at gas outlet. In addition, if we consider that the ageing process have caused a liquid water accumulation inside the stack, the decrease in each cell performances and the enhancement of the

performance differences can be easily explained. Indeed, as can be seen from Eqs. (3), (6) and (8), an increase in the water content causes a decrease in the GDL porosity and thus a slower diffusion of the gases. This in turn increases the voltage losses by mass transfer limitation, as shown by our simulation results that indicate a strong and rapid decrease of the oxygen pressure at the GDL/electrode interface (Fig. 10).

In addition, beyond a critical water content, the apparent exchange current density is also affected by water accumulation: the values of j_{eq} that correctly fit our experimental results in the case of the aged stack is about 10 times lower than the one obtained by the fitting of the results obtained for the fresh stack. Such decrease in the actual exchange current density can be explained by a change in the accessibility of the active surface for the oxygen gas. Even if our simple model has not taken into account the complex structure of the active layer, it can be stated that liquid water partly fills the gas pore of the AL too. Diffusion path of dissolved oxygen in this layer is thus increased. In turn, diffusion limitation is increased, leading to a smallest effective equilibrium current density [31].

Finally, the very high values of the liquid water content (between 82 and 85%) that allow us to correctly fit our experimental results indicate that the water management issue in a fuel cell operating in dead-end mode is mainly associated with pore flooding while the risk of a membrane drying by insufficient amount of water seems unlikely. As a consequence, the inlet gases humidification seems to be unnecessary to guarantee a good fuel cell performance during operation in dead-end mode.

6. Conclusions

The voltage evolution of a fuel cell operating in dead-end mode after a current step exhibits two different response times: one at about 40 ms, corresponding to the charge of the double-layer capacitance and the other one at about 15–20 s. The first time constant is independent of the stack's history but the corresponding voltage level is strongly impacted. An influence of the cell's position in the stack on its performance has also been observed: the cell located at the gases inlet exhibits better performances than the one located at the dead-end. This difference was explained by a water accumulation at the outlet and by higher gases partial pressure at the cell located in gases inlet. The differences between the cell performances are enhanced by the ageing.

The one-dimensional model we have developed is able to fit our experimental results with a good accuracy. The only observed discrepancies are linked with physical phenomena that were not taken into account in our model (increase in temperature by Joule effect and water distribution in the membrane) or to its simplification (the volumic structure of the active layer was not taken into account). Our model indicated that, even a fresh cell contains a high amount of liquid water when stored at room temperature and that the cell performance was rapidly limited by oxygen mass transport inside the GDL. Further experimental and simulation studies will be performed to improve the prediction's accuracy of the model and to better understand the water management effect in a fuel cell operating in dead-end mode.

Acknowledgements

The authors would like to thank the French Ministries of Research and Industry for their financial support.

References

[1] J. Larminie, A. Dicks, Fuel Cell Systems Explained, 2nd ed., John Wiley and Sons, 2003.
[2] D.M. Bernardi, J. Electrochem. Soc. 137 (11) (1990) 3344–3350.
[3] T.V. Nguyen, R.E. White, J. Electrochem. Soc. 140 (8) (1993) 2178–2186.
[4] T.E. Springer, T.A. Zawodzinski, S. Gottesfeld, J. Electrochem. Soc. 138 (8) (1991) 2334–2342.
[5] G. Murgia, L. Pisani, M. Valentini, B.D. Aguanno, J. Electrochem. Soc. 149 (1) (2002) A31–A38.
[6] D.M. Bernardi, M.K. Verbrugge, J. Electrochem. Soc. 139 (9) (1992) 2477–2491.
[7] T.E. Springer, M.S. Wilson, S. Gottesfeld, J. Electrochem. Soc. 140 (12) (1993) 3513–3526.
[8] J.S. Yi, T.V. Nguyen, J. Electrochem. Soc. 146 (1) (1999) 38–45.
[9] D. Natarajan, T.V. Nguyen, J. Electrochem. Soc. 148 (12) (2001) A1324–A1335.
[10] N. Wagner, J. Appl. Electrochem. 32 (8) (2002) 859–863.
[11] M. Cearolo, C. Miulli, A. Pozio, J. Power Sources 113 (2003) 131–144.
[12] S. Yerramalla, A. Davari, A. Feliachi, T. Biswas, J. Power Sources 124 (2003) 104–113.
[13] W. Friede, S. Raël, B. Davat, IEEE Trans. Power Electron. 19 (5) (2004) 1234–1241.
[14] Y. Wang, C.Y. Wang, Electrochim. Acta 50 (2005) 1307–1315.
[15] F. Chen, H.-S. Chu, C.-Y. Soong, W.-M. Yan, J. Power Sources 140 (2005) 243–249.
[16] Y. Shan, S.-Y. Choe, J. Power Sources 145 (2005) 30–39.
[17] P.R. Pathapati, X. Xue, J. Tang, Renew. Energy 30 (2005) 1–22.
[18] S. Shimpalee, W.-K. Lee, J.W. Van Zee, H. Naseri-Neshat, J. Power Sources 156 (2006) 355–368.
[19] S. Shimpalee, W.-K. Lee, J.W. Van Zee, H. Naseri-Neshat, J. Power Sources 156 (2006) 369–374.
[20] J. Garnier, J.-P. Diard, M.C. Péra, F. Harel, D. Candusso, D. Hissel, N. Glandut, A. De Bernardinis, J.-M. Kauffmann, G. Coquery, IEEE Semin. 1 (2003), ISBN 0-7803-7955-1.
[21] M. Bautista, Y. Bultel, P. Ozil, Trans. IChemE, Part A 82 (A7) (2004) 907–917.
[22] S. Kim, S. Shimpalee, J.W. Van Zee, J. Power Sources 135 (2004) 110–121.
[23] S. Kim, S. Shimpalee, J.W. Van Zee, J. Power Sources 137 (2004) 43–52.
[24] S. Kim, S. Shimpalee, J.W. Van Zee, J. Electrochem. Soc. 152 (6) (2005) A1265–A1271.
[25] R.B. Bird, W.E. Stewart, E.N. lightfood, Transport Phenomena, John Wiley and Sons, New York, 1960.
[26] R.H. Perry, D.W. Green, J.O. Maloney, Perry's Chemical Engineers' Handbook, Mc Graw Hill, New York, USA, 1984.
[27] S. Mazumder, J.V. Cole, J. Electrochem. Soc. 150 (11) (2003) A1510–A1517.
[28] D.A.G. Bruggeman, Ann. Phys. (Leipzig) 24 (1935) 636.
[29] A. Parthasarathy, S. Srinavasian, A.J. Appleby, J. Electrochem. Soc. 139 (1992) 2530–2537.
[30] A.J. Bard, L.R. Faulkner, Electrochemical Methods: Fundamentals and Applications, 2nd ed., John Wiley and Sons, 2001.
[31] Y. Bultel, K. Wiezell, F. Jaouen, P. Ozil, G. Lindbergh, Electrochim. Acta 51 (2005) 474–488.
[32] U. Pasaogullari, C.Y. Wang, J. Electrochem. Soc. 151 (3) (2004) A399–A406.